atmosphere

Article

Intra-Seasonal Features of Winter Extreme Cold Events in Northeast–North China and Synergistic Effects of Circulation Systems in Mid-High Latitude

Qingjiu Gao *, Li Wang, Yan Li and Yafei Wang

Key Laboratory of Meteorology Disaster, Ministry of Education (KLME), Joint International Research Laboratory of Climate and Environment Change (ILCEC), Collaborative Innovation Center on Forecast and Evaluation of Meteorological Disasters (CIC-FEMD), Nanjing University of Information Science & Technology, Nanjing 210044, China

* Correspondence: gaoqj@nuist.edu.cn

Abstract: Based on the daily minimum air temperature (T_{min}) data from the China Meteorological Data Network and the NCEP/DOE reanalysis data, the intra-seasonal circulation characteristics and evolution of extreme cold events (ECEs) in Northeast–North China (NE-N) during the winter of 1979–2018 are explored, and the synergistic effects of key circulation systems in the mid-high latitude on ECEs are discussed. The results show that: (1) the winter daily T_{min} in the NE-N region presents a significant low-frequency period of 10–30 d; during the cooling phases, a pair of cyclone–anticyclone in the lower troposphere moves southeastward, accompanying the intensifying Siberian High, and leads to the abnormal northerly; the developing wave trains in the middle troposphere result in enhancing and maintaining cold air; furthermore, the situation of the upper tropospheric jet weakening in the north and strengthening in the south is favorable for cold air to move southward and accumulate in the NE-N region. (2) There are two wave trains in the Eurasian at 200 hPa level. The north one moves southeastward through the Ural Mountains to the coast of East Asia, with the upstream wave activity flux dispersing to NE-N region, causing the northeast cold vortex to develop. The south one with relatively weak intensity disperses the wave flux northward, and enhances the cold vortex. (3) The key circulation systems of ECEs are the Siberian High, the Ural Mountain Blocking High, the Northeast Cold Vortex, and the East Asian Subtropical Jet. The Ural Mountains Blocking High leads four phases earlier than low temperature, and the rest of the systems are basically in phase with low temperature. The synergistic effect of circulation systems will lead to extended-range cold in the NE-N region.

Keywords: extreme cold events; intra-seasonal oscillation (ISO); mid-high latitude circulation systems; synergistic effect; wave activity flux

check for updates

Citation: Gao, Q.; Wang, L.; Li, Y.; Wang, Y. Intra-Seasonal Features of Winter Extreme Cold Events in Northeast–North China and Synergistic Effects of Circulation Systems in Mid-High Latitude. *Atmosphere* **2022**, *13*, 1425. https://doi.org/10.3390/atmos13091425

Academic Editor: Graziano Coppa

Received: 10 August 2022
Accepted: 30 August 2022
Published: 2 September 2022

1. Introduction

Some recent studies suggested that the frequency and intensity of extreme weather events increase due to the significant global climate change; thus, extreme cold events (ECEs) and related secondary disasters present a more serious state [1,2]. As the political, transportation, and agricultural center of China, cold surges have tremendous damage on the economy and people's lives in Northeast and North China (NE-N), the disastrous events attract broad attention from society.

The direct reason for ECEs is the abnormal atmospheric circulation. As one of the most active circulation systems in the Northern Hemisphere during winter [3], studies show that the strength of the East Asian winter monsoon leads to unusual temperature in China [4,5]. The members of the winter monsoon system mainly include the Siberian High (SH), the Ural Blocking High (UBH), the East Asian Trough, and the westerly jet in the upper troposphere [6–8]. Besides the effects of the individual system only, recent studies pointed out that the synergistic effect of each system can cause extended persistent cold events in China. The interaction of UBH and SH will have a more significant impact on the wind and temperature fields in winter [9–11]; the Arctic Oscillation (AO) is related to the tropospheric circulation system through westerly disturbances in the lower stratosphere at mid-high latitude, causing the SH in phase with the Aleutian Low, further leading to a steep temperature anomaly in East Asia [12–14]; the synergistic effect of high-latitude blocking often causes ECEs in China by transiting the AO phase, Polar Vortex intensity, and location, which provides a reference for predicting ECEs about 10–20 days ahead [15].

The intra-seasonal oscillation (ISO) mainly includes two concerned bands with 10–30 d and 30–60 d periods, which are between the weather and short-term climate change, and have a profound influence on persistent circulation anomalies and the local weather and climate [16,17]. Earlier research mainly focuses on the phenomenon over tropical regions [18–20]; however, ISO is found on a global scale [21,22]. More recent studies demonstrate that ISO over mid-high latitude plays a critical role in precipitation and temperature anomalies [23–25], and also provides a favorable large-scale circulation for cold surges [26,27].

The winter temperature in China and related mid-high latitude circulation systems also have robust ISO periods. The strong cold air mainly manifests a quasi-40 d periodic oscillation [28], and the interaction of ISO between mid-high and low latitudes will provoke the outbreak of persistent ECEs in China [29–31]. Many case studies pointed out that Chinese winter temperatures, SH, and the mid-high latitude blocking high show a significant ISO period of 10–30 d. The intra-seasonal evolution of the UBH is favorable for enhancing SH, and, thus, result in the cold wave intensifying [32,33]; the Northeast-Asian-type Polar Vortex is most closely related to winter temperature in Northeast China. Both the geopotential height in the key stratosphere and the surface temperature in Northeast China have an oscillation period of about 50 d, and the ISO of the geopotential height is ahead of the temperature [34], which is an indicator for the medium-range forecasting of persistent low temperature processes [35,36].

Previous works investigated the causes of extreme low temperature on an intra-seasonal scale; the studies mainly focus on individual circulation systems and cases, but how they synergistically affect ECEs has yet to be fully elucidated. Therefore, this paper intends to explore the internal mechanism of occurrence and development of ECEs in NE-N through the synergistic effects of various systems, with a view to provide a theoretical basis for extracting extended-term forecast signals.

The rest of the paper is organized as follows. Section 2 describes the data and methodology. Section 3 defines the low-temperature threshold and extended persistent cold events in the NE-N region; Section 4 discusses the ISO characteristics of ECEs, and identifies the key circulation systems; Section 5 explores the synergistic variation of the systems and their effects on low-frequency ECEs (LECEs) in the NE-N region. Section 6 provides a summary and discussion of the full text.

2. Data and Methodology

2.1. Data

The daily minimum temperature (T_{min}) is obtained from China's Ground Temperature 0.5° × 0.5° Gridded Dataset (V2.0), provided by The National Climate Center of China Meteorological Administration (NCC/CMA). The dataset is compiled from the daily temperature records of 2472 meteorological stations (excluding 2 distant island stations) over the Chinese mainland [37,38]. The National Meteorological Information Center organizes the data and conducts strict checks and audits. Gridded data is interpolated from station data using Thin Plate Spline and 3D geospatial information. The cross-validation results show that the interpolation model gets a good effect, and the precision is relatively high [39], so T_{min} can be used to analyze the low temperature characteristics.

The daily reanalysis data, with a resolution of 2.5° × 2.5° and 17 vertical pressure levels (1000–10 hPa), is provided by the National Centers for Environmental Prediction/Department of Energy (NCEP/DOE) [40]. The variables include sea level pressure (SLP), geopotential height, temperature, vertical p-velocity, and zonal and meridional wind.

The data for this study span from 1979 to 2019, with winter defined as December, January, and February (February 29 in leap years is removed from the data). The NE-N region is between 35–55° N and 110–135° E within China.

2.2. Methods

To identify the dominant oscillation period of T_{min} in the study area, a power spectrum analysis and red noise test are performed after removing the annual cycle and synoptic-scale disturbance (7-day running mean). The intra-seasonal components of meteorological elements are extracted accordingly by a Lanczos band-pass filter [41], and then we find essential circulation systems by elaborating the circulation features of LECEs through composite analysis. Moreover, methods such as lead-lag correlation analysis and Student's *t*-test are also used in this paper [42–44].

The propagation of wave energy can be well described by the T-N wave activity flux; the two-dimensional horizontal expression is as follows [45,46]:

$$W = \frac{p\cos\varphi}{2|\mathbf{U}|}\begin{pmatrix} \frac{U}{a^2\cos^2\varphi}\left[\left(\frac{\partial\psi'}{\partial\lambda}\right)^2 - \psi'\frac{\partial^2\psi'}{\partial\lambda^2}\right] + \frac{V}{a^2\cos\varphi}\left[\frac{\partial\psi'}{\partial\lambda}\frac{\partial\psi'}{\partial\varphi} - \psi'\frac{\partial^2\psi'}{\partial\lambda\partial\varphi}\right] \\ \frac{U}{a^2\cos^2\varphi}\left[\frac{\partial\psi'}{\partial\lambda}\frac{\partial\psi'}{\partial\varphi} - \psi'\frac{\partial^2\psi'}{\partial\lambda\partial\varphi}\right] + \frac{V}{a^2}\left[\left(\frac{\partial\psi'}{\partial\varphi}\right)^2 - \psi'\frac{\partial^2\psi'}{\partial\varphi^2}\right] \end{pmatrix} \tag{1}$$

where U, V are the meridional and zonal winds of the background field (winter 1979–2018), $|\mathbf{U}| = \sqrt{U^2 + V^2}$; ψ' is the low-frequency quasi-geostrophic perturbation stream-function relative to the background field; φ, λ denote the latitude and longitude, respectively; a represents the earth's radius; and $p = (pressure/1000\text{ hPa})$.

To discuss the synergistic effect of the key circulation systems on LECEs by their variation and configuration, the strength indexes are defined as follows [47–49]:

(1) Siberian High Index (SHI): the regional mean SLP anomaly averaged over the area, 40–65° N and 80–120° E, in the extended winter season (from October to March of the next year);
(2) Ural Blocking High Index (UBHI): the regional mean geopotential height anomaly at 500 hPa averaged over the area, 50–70° N and 55–80° E, in the extended winter season;
(3) Northeast Cold Vortex Index (NECVI): the regional mean geopotential height anomaly at 500 hPa averaged over the area, 40–50° N and 120–130° E, in the extended winter season;
(4) East Asian Subtropical Jet Index (EASJI): the regional mean zonal wind anomaly at 300 hPa averaged over the area, 30–37.5° N and 120–150° E, in the extended winter season.

3. Definition of ECEs

In this paper, the percentile method is applied to calculate the low temperature threshold [50]: the extreme low temperature threshold for the grid point on a given calendar day is the 10th percentile value of T_{min} in ascending yearly order (the percentile for the day was calculated using five-day windows centered on that day across all years). In order to identify typical ECEs, the threshold of its winter averaged is taken as the criterion for judging low-temperature days (T_{min} is lower than the winter-average threshold). The spatial distribution of the daily average threshold value is shown in Figure 1. The 0 °C line nears 25° N, with a negative zone to its north (except for the Sichuan Basin) and a positive zone to its south. The lowest temperature in Northeast China can reach below −36 °C.

The following criteria are used to determine a ECE in the NE-N region [50,51]:

(1) Low temperature day: T_{min} is lower than the winter-average threshold;
(2) The number of grid points meeting the low temperature day is counted as the extreme cold area index S for that day. S constitutes at least 17.48% of the total grid number of NE-N, and the maximum S exceeds 34.96% of the total grid number of NE-N;

(3) Persistence: persisting for more than eight days (maximum interruptions of two days are allowed).

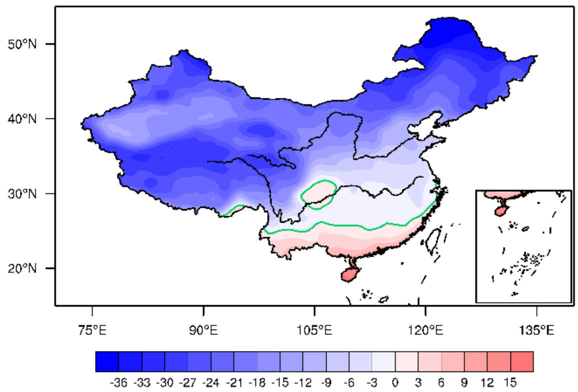

Figure 1. Spatial distribution of winter-averaged low-temperature threshold (green contour denotes the 0 value, unit: °C).

According to this, a total of 42 ECEs in NE-N are identified, and the frequency displays obvious interannual anomaly characteristics. In the winters during 1985 and 2000, three ECEs with the highest number occurred; the winters during 1979–1986 are the period of frequent ECEs, with an average of 1.88 events per year; there is an apparent decrease from 1987–1995, with an average of 0.44 events per year, and then an increase again from 1996–2018, with an average of 1 event per year. This is consistent with the conclusions obtained by Shi [52] and Xu [53].

4. Intra-Seasonal Oscillation Features of ECEs

4.1. Determination of LECEs

A power spectrum analysis of T_{min} in the NE-N region during the winters of 1979–2018 (Figure 2a) reveals that it passes the 95% red noise test in the 10–40 d band, and there is a significant spectral peak near 30 d. It can be seen from Figure 2b that the standard deviation of T_{min} after 10–30 d filtering in the NE-N area is relatively high, and it can exceed 2 °C in most areas. The standard deviation of the regional averaged T_{min} before and after filtering was calculated separately, and the contribution rate of the 10–30 d intra-seasonal component was 44.96%, indicating that there is a large 10–30 d variability of T_{min} in NE-N; thus, LECEs will be defined based on this.

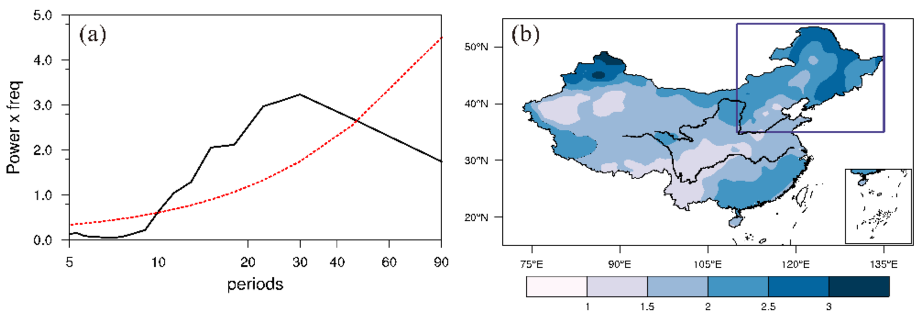

Figure 2. (**a**) Winter mean power spectra of daily T_{min} over the NE-N region (solid black line) during 1979–2018. The dashed red line represents the 95% significant level of red noise spectrum. (**b**) Standard deviation of 10–30 d filtered T_{min} (unit: °C) in winter. The box denotes the NE-N region (35–55° N, 110–135° E).

The 10–30 d Lanczos band-pass filter is performed on the T_{min} minus threshold in the NE-N region from 1979 to 2019. Taking the winter of 2000 as an example (Figure 3), the variation of the cold days corresponds well to the 10–30 d filtered temperature series, and the transition phase from positive to negative meets with the unfiltered series. Dividing each fluctuation of the filtered temperature into eight phases, phase 1 (5) is the transition phase from negative (positive) to positive (negative), phase 3 (7) is the peak (valley) phase, and the amplitude values of phases 2, 4 (6, 8) are half of the wave peaks' (valleys').

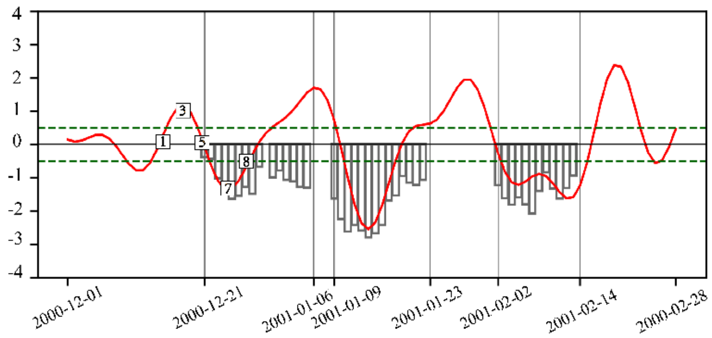

Figure 3. Time series of T_{min} minus threshold (grey bar, unit: °C) and standardized 10–30 d filtered T_{min} (red line) averaged over the NE-N during the winter in 2000 (green dashed line represents 0.5 standard deviation; between the two vertical lines is an ECE; the numbers, 1, 3, 5, 7, and 8, represent the different phases of the ISO).

The amplitude of the normalized filter sequence exceeding ±0.5 standard deviation is recorded as a LECE. There are 31 events with 10–30 d ISO characteristics finally selected from the 42 ECEs, and the specific dates of their peak phase (phase 3) and valley phase (phase 7) are shown in Table 1.

Table 1. The specific dates of peak phase (phase 3) and valley phase (phase 7) of 31 LECEs in the NE-N region.

Case	Phase 3	Phase 7	Case	Phase 3	Phase 7
1	1979/12/31	1980/01/16	17	2000/12/18	2000/12/24
2	1980/12/20	1981/01/02	18	2001/01/06	2001/01/14
3	1981/01/10	1981/01/16	19	2002/12/17	2003/01/02
4	1981/12/23	1981/12/29	20	2006/01/27	2006/02/04
5	1982/01/09	1982/01/16	21	2009/12/23	2009/12/31
6	1984/01/11	1984/01/17	22	2010/01/06	2010/01/13
7	1984/01/28	1984/02/05	23	2011/01/21	2011/01/28
8	1985/01/03	1985/01/14	24	2012/01/17	2012/01/26
9	1985/12/02	1985/12/09	25	2012/12/15	2012/12/23
10	1985/12/27	1986/01/03	26	2013/02/01	2013/02/07
11	1986/12/24	1986/12/30	27	2014/01/03	2014/01/13
12	1987/01/05	1987/01/11	28	2016/01/14	2016/01/20
13	1993/01/03	1993/01/16	29	2018/01/18	2018/01/24
14	1996/12/26	1997/01/05	30	2018/12/21	2018/12/28
15	1998/01/10	1998/01/23	31	2019/02/01	2019/02/09
16	1999/12/27	2000/01/05			

4.2. Features of Intra-Seasonal Circulation

After removing the annual cycle and synoptic-scale fluctuations, the 10–30 d band-pass filtering is applied to the daily reanalysis data to analyze the tropospheric circulation structure and investigate the primary low-frequency circulation systems.

4.2.1. Structure and Evolution of Horizontal Circulation

Figure 4 presents the synthetic evolution of the 10–30 d filtered temperature at a 925 hPa level, and the wind at an 850 hPa level. The temperature anomalies in Northeast

China are all positive and increasing during the warming phases (phases 1–3); phase 4 is the transition phase, the center of the positive temperature anomalies moves southeastward; the NE-N region is covered by negative temperature anomalies in phases 5–7, and reaches the strongest in phase 7. It is clear from the wind field that over the mid-high latitude, there is an abnormal cyclone during phases 1–2, and a strong anticyclone close to the Kara Sea in phase 3. Afterward, the anticyclone gradually moves to the southeast, and the cyclonic circulation near the northeast of China is more obvious (phases 4–6); thus, the anomalous northerly component between the anticyclone and the northeast cyclone is stronger. Under the influence of persistent northerly airflow, more cold air from high latitude is advected and converges in the NE-N region at phase 7, resulting in the temperature dropping to the minimum. At phase 8, the anomalous anticyclone disappears, and the cold center also moves out of the NE-N region.

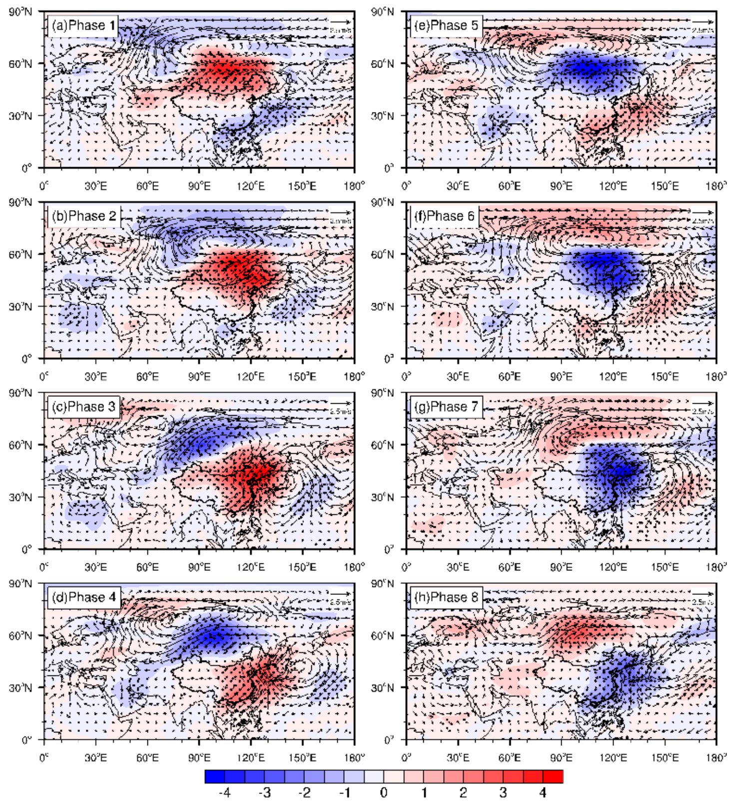

Figure 4. Phase evolution of 10–30 d filtered 925 hPa temperature (shading; unit: °C) and 850 hPa wind (vector; unit: m/s) of LECEs ((**a**–**h**), dotted area passes the 95% significance level).

The phase evolution of the 500 hPa vorticity and SLP for LECEs is shown in Figure 5. The negative vorticity anomaly locates near Novaya Zemlya in the early stage of cooling (phases 1–2), and the negative vorticity anomaly expands in phases 3–4 and moves southeastward to the Ural Mountains, which represents the development of UBH; by this time, the Baikal region is controlled by the positive vorticity anomaly, and, in its downstream, an anticyclonic anomaly exists stably, whereas a "− + −" wave train was formed from the Ural Mountains to the Sea of Okhotsk, and the center of the wave train moves southeastward while intensifying. The positive anomaly of SLP locates in West Siberia, and then gradually expands and controls most of China at phase 6. The SH situates more southward and more eastward, and the center of the positive vorticity anomaly moves to 120° E, corresponding to the formation and maintenance of the Northeast Cold Vortex (NECV), which is favorable for cold air to invade China from the west of low pressure. The negative vorticity anomaly over the Sea of Okhotsk tends to be favored for the cold vortex stagnant in NE-N. The range of the positive anomaly in the SLP shrinks at phase 7; Northeast Asia and the coastal areas of East Asia are controlled by negative SLP anomalies, and the northerly airflow between them carries cold air from Central Siberia to the northeast, which further reduces the temperature in the NE-N region (Figure 5g). The center of the cold vortex moves out of China to the Sea of Japan in phase 8, and the cooling process tends to end with the weakening and contraction of SH.

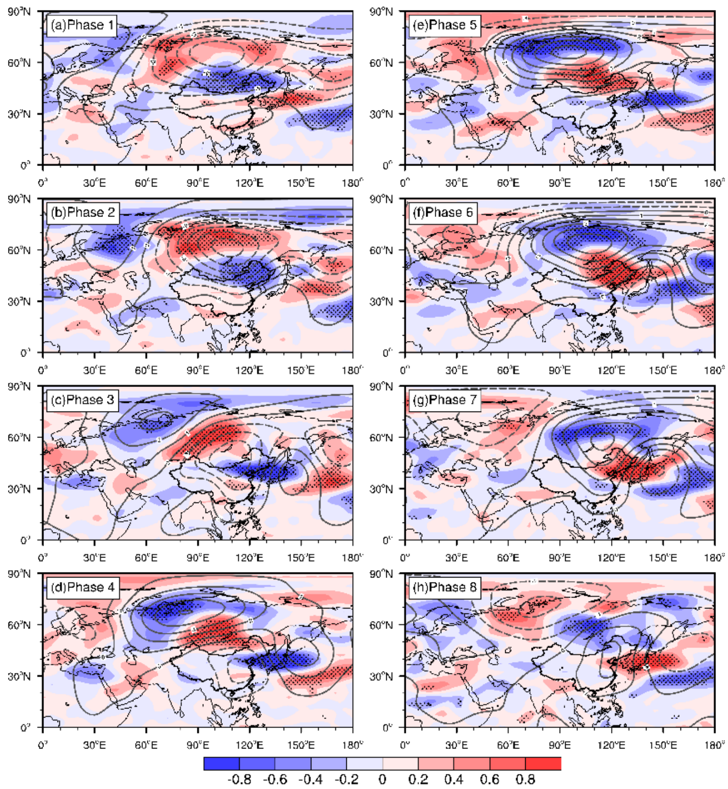

Figure 5. Phase evolution of 10–30 d filtered 500 hPa vorticity (shading; unit: 10^5 s^{-1}) and SLP (contour; unit: hPa) of LECEs ((**a**–**h**), dotted area passes the 95% significance level).

The observational analyses suggest the circulation system in mid-low troposphere is characterized by eastward movement. In the cooling phases (phases 5–7), the SH expands to the southeast; at the same time, the 500 hPa vorticity presents the features of "two ridges and one trough": negative vorticity anomalies lie near the Ural Mountains and the Yakutsk region, while a positive anomaly lies in the NE-N region, corresponding to the inverse Ω pattern of the geopotential height field. Under the influence of the East Asian Trough, the northerly airflow in front of the ridge and behind the trough guides the low-level cold air southward to invade China, which is conducive to temperature reduction. In conclusion, NECV and UBH in the mid-troposphere and SH in the SLP are the key systems affecting ECEs.

As one of the members of the East Asian monsoon, the East Asian upper tropospheric jet is associated with the temperature anomalies in East Asia. It is proved that the temperate jet is stronger at 300 hPa, whereas the strength of subtropical jet is comparable at 300 hPa and 200 hPa [54]. Therefore, the winter-averaged zonal wind field of 300 hPa from 1979 to 2018 was calculated (not shown). Besides the large-value area observed in the western North Pacific and south of Japan, usually named the East Asian Subtropical Jet (EASJ) area, there is also a large zonal wind speed area to the east of Lake Baikal called the East Asian Polar Front Jet (EAPJ) area. The correlation analysis between the areal-averaged (T_{min} minus threshold) $\times$ (-1) and 300 hPa zonal wind field in phase 7 (not shown) indicates that the EAPJ area presents a negative correlation, whereas the EASJ area presents a stronger and more significant positive correlation.

The evolution of the zonal wind at 300 hPa (Figure 6) depicts that in the early period (phases 1–3), Lake Baikal and its vicinity are occupied by a stronger upper-level jet; hence, the cold air is blocked at high latitudes; then, cold air moves southward, accompanied by the positive anomaly of the jet moving to Northern China. The weak EAPJ during phases 6–7 favors the invasion of cold air from high latitudes into China through Lake Baikal, whereas the strong EASJ causes cold air to accumulate in NE-N, resulting in further temperature reduction. Therefore, the barrier effect of EASJ is closely linked to low temperature, and is a key circulation system in the upper troposphere.

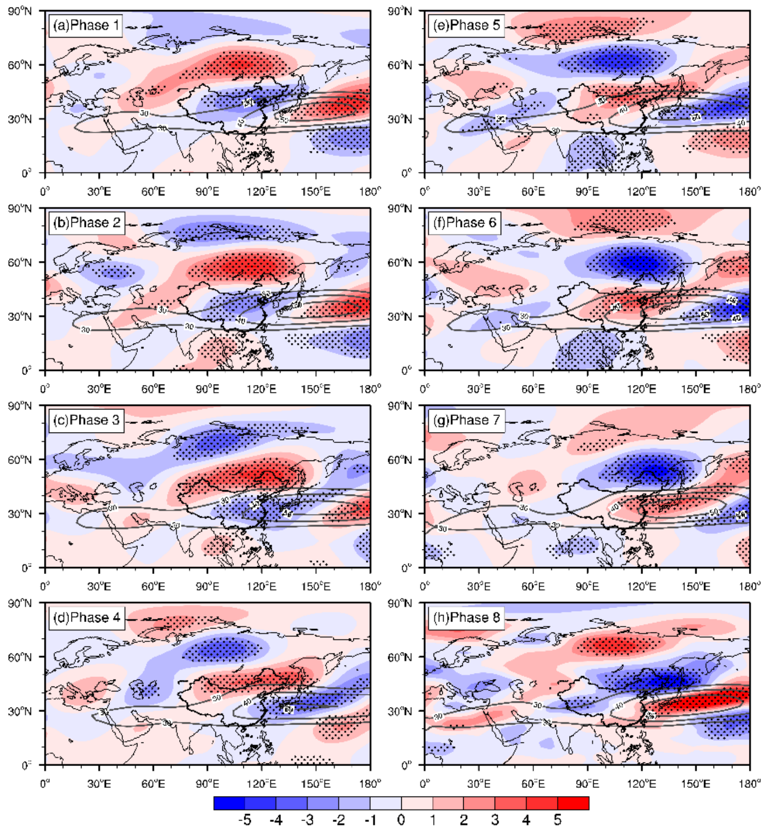

Figure 6. Phase evolution of 300 hPa zonal wind (shading: 10–30 d filtered; contour: unfiltered; unit: m/s) of LECEs ((**a**–**h**), dotted area passes the 95% significance level).

4.2.2. Propagation of Wave Activity Flux

The above analysis demonstrates that the evolution of the circulation system may lead to the development and occurrence of LECEs, and what are the reasons? We try to discuss it from the perspective of wave activity flux.

It can be seen from Figure 7 that there are two northwest–southeast-oriented wave trains in the Eurasian continent, named after the northern and southern branch, respectively. The northern one propagates along the path of the Barents Sea–Kara Sea–West Siberia–NE-N region. The southern one propagates along the path of the Western European continent–the Middle East–the Bay of Bengal. Both wave trains propagate southeastward, reflecting the propagation path of energy in ECEs. The wave activity flux of the northern branch is significantly enhanced in phase 6–7, and the influence extent is expanded, which laterally reflects the greater influence of the northern wave train on ECEs in the NE-N region.

The "+ − +" wave train pattern on the 200 hPa quasi-geostrophic perturbation streamfunction (shading in Figure 7) is similar to that of the 500 hPa vorticity (shading in Figure 5). The negative center during phases 1–4 moves from the Ural Mountains to Lake Baikal with a gradual decrease extent; later, the intensity increases, corresponding to the advance of the cold vortex. The wave activity flux manifests a strong convergence over NE-N during phases 6–7, with the wave energy deepening the NECV and local circulation anomaly. The obstruction of the downstream blocking high is beneficial to maintain the NECV, and to confine cold air to NE-N. By contrast, the intensity of the low-latitude signal represented by the southern wave train is weaker, and the wave flux is transmitted northeastward to develop the NECV during phases 2–6.

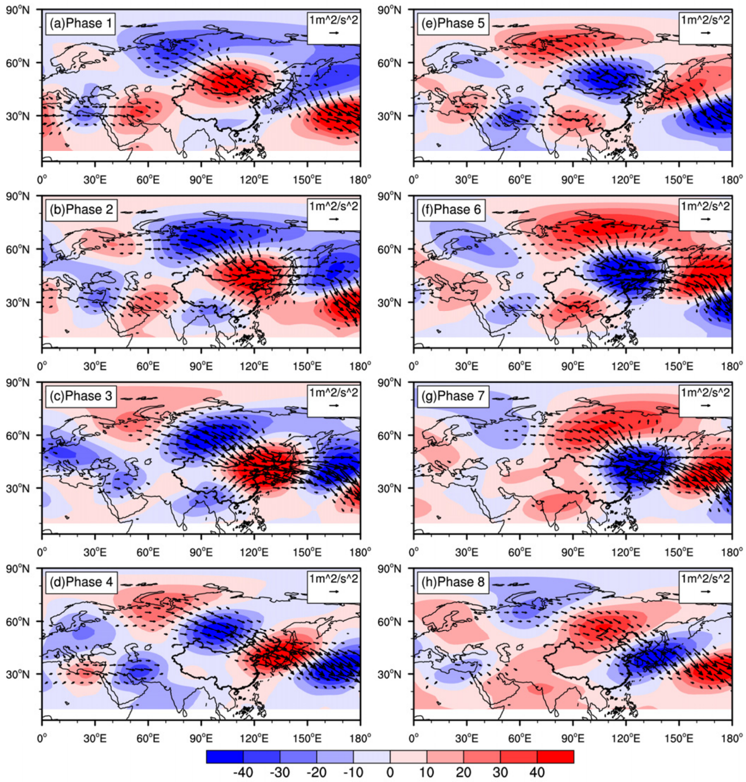

Figure 7. Phase evolution of 10–30 d filtered 200 hPa T-N wave activity flux (vector; unit: m^2/s^2; values less than 0.3 m^2/s^2 are masked) and quasi-geostrophic perturbation stream-function (shading; unit: 10^{-5} m^2/s) of LECEs.

4.2.3. Structure and Evolution of Vertical Circulation

The analysis of the tropospheric horizontal circulation shows that the evolution of LECEs in winter in the NE-N region is mainly characterized by cold anomalies and the southward propagation of the cold vortex. This feature is more obvious in the vertical profiles of 10–30 d filtered height and temperature fields (Figure 8). The negative temperature anomalies in the incipient stage (phases 1–2) are mainly concentrated in the stratosphere and upper troposphere, whereas the cold anomaly at the low level is weaker and situates more northward. The geopotential height anomaly in the troposphere is negative in the north and positive in the south, with 55° N as the dividing line. Then, the cold vortex in the high latitude of the stratosphere descends and moves southward during phases 3–5, guiding the cold air to spread southward and downward; thus, the scope of the low-level cold anomaly gradually expands. Simultaneously, the northeast region is controlled by the ascending motion, and adiabatic cooling is beneficial to the reduction of the temperature in the later period. The geopotential height anomaly evolves into a north–positive and south–negative distribution during phases 6–7, and the cold vortex also moves southward to the northeast, where it is controlled by a deep low-pressure system that favors the excitation of northerly wind anomalies. The temperature anomaly exhibits a structure of upper–warm and lower–cold, with the center of the tropospheric cold anomaly strengthening and moving southward, contributing to the lower temperature in the NE-N region.

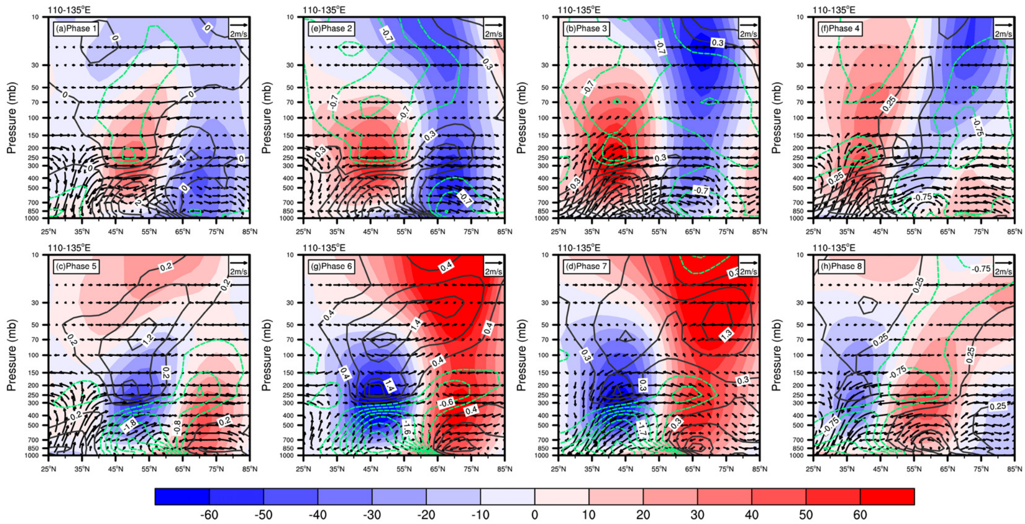

Figure 8. The vertical-meridional cross section of 10–30 d filtered geopotential height (shading; unit: gpm), temperature (contour; unit: °C; green contours indicate the negative values), and wind (vector; meridional wind unit: m s^{-1}, vertical velocity unit: -10^2 Pa s^{-1}) averaged along the longitudes 110–135° E during LECEs.

5. Synergistic Variation of Intra-Seasonal Circulation Systems

As discussed previously, the key systems affecting the low temperature events in the NE-N region include SH, UBH, NECV, and EASJ. The quantitative indexes mentioned in Section 2.2 are used to explore the key systems' intra-seasonal characteristics.

The power spectral analysis of each index (Figure 9) shows that SH, UBH, and EASJ display 10–60 d ISO periods, and NECVI displays 10–40 d periods. All of them have significant spectral peaks within 10–30 d and pass the 95% red noise test. Based on this, 10–30 d band-pass filtering is performed to analyze the intra-seasonal variation features, and the effect of their synergy on ECEs is discussed through the periodic variation.

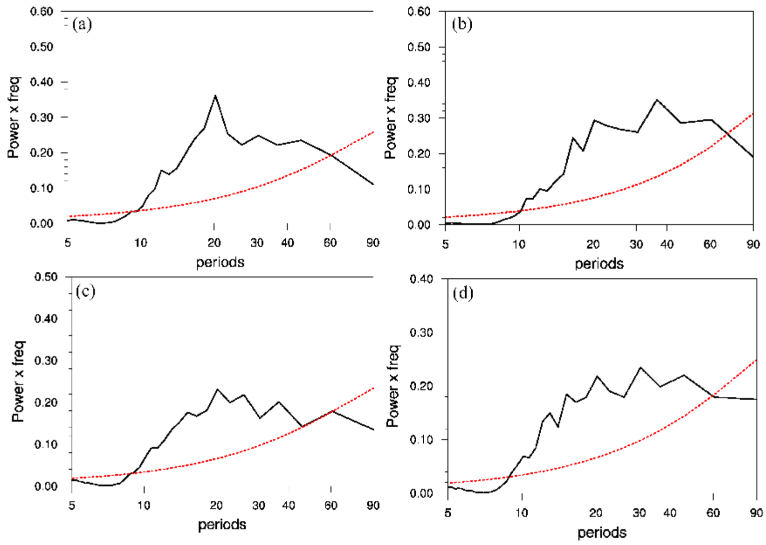

Figure 9. Power spectra of (**a**) SHI, (**b**) UBHI, (**c**) NECVI, and (**d**) EASJI (solid black line). The dashed red line represents the 95% significant level of the red noise spectrum.

As depicted in Figure 10a, each system is weak in the incipient stage, whereas the UBHI in the middle troposphere is stronger in phases 4–5, leading four phases earlier than low temperature. The NECVI peaks in phase 6, and advances the low temperature by one phase due to the eastward UBH. SHI is stronger in phases 5–6, and leads two phases earlier than low temperature, and the intensity is slightly lower than other systems in the mid-troposphere. EASJI gradually increases after phase 4 and reaches a peak value in phase 7, inducing a cold air confine in North China, which further reduces the temperature in the NE-N region.

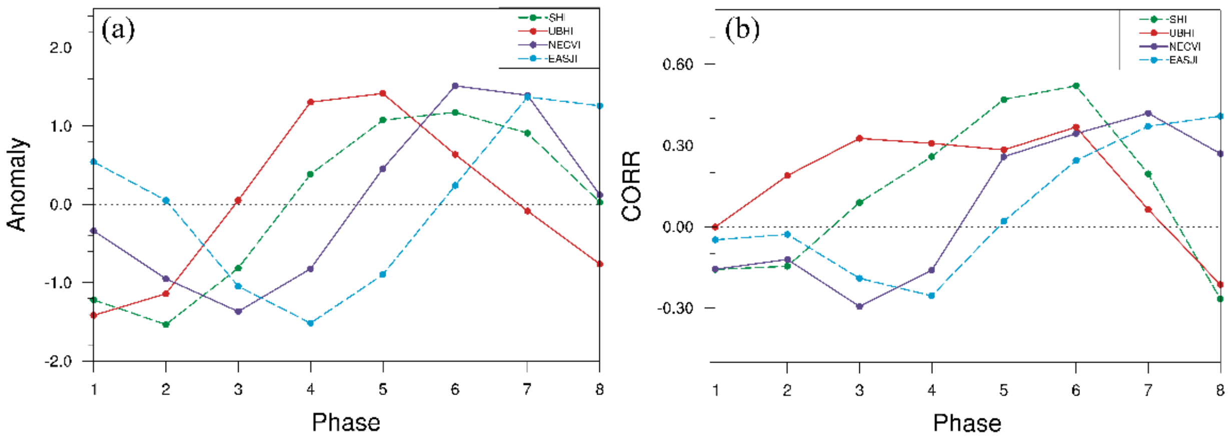

Figure 10. Phase evolution of (**a**) the strength indexes and (**b**) lead-lag correlation coefficients between strength indexes at phases 1–8 and (T_{min} minus threshold) × (−1) at phase 7.

The results of the lead-lag correlation analysis between the circulation system indexes in each phase and the (T_{min} minus threshold) × (−1) in phase 7 (Figure 10b) reveal that the positive correlation coefficient of UBHI is higher in phase 3 (leads four phases); that is, the development of UBH in the early stage favors the reduction of temperature in the later stage. The highest correlation coefficient of UBHI appears in phase 6 (leads one phase), whereas both NECVI and SHI have higher correlation coefficients with low temperature; SHI even reaches 0.52 (passing the 95% confidence level). This indicates that the synergistic effect of UBH, SH, and NECV will cause prevailing northerly winds, and transport cold air over Northern China in conjunction with EASJ, significantly correlated with the low temperature at phases 7–8, which is favorable for maintaining the NECV and accumulating cold air, provoking persistently low temperatures in the NE-N region.

As mentioned above, the synergistic variation of the circulation systems in the upper and lower levels are conducive to the occurrence of LECEs in the NE-N region. As we can see from the configuration of the circulation systems during the cooling process (Figure 11), the cold air is initially located near Novaya Zemlya at high latitudes, and the strong EAPJ obstructs the cold air moving southward and accumulating in the mid-high latitudes; the circulation in the Eurasian region has a strong meridional component, and exhibits an inverse Ω pattern with "two ridges and one trough" at 500 hPa. By this time, the cold vortex is located to the west of Lake Baikal, and the northerly airflow behind the east–west-oriented trough and the southwest of the cold vortex transports cold air to the north of the Sayan Range. Moreover, the Siberia region of the SLP is a negative anomaly. The NE-N region is a warm anomaly and is not affected by cold air. With the evolution of ISO phases, the weakening of the upper-level EAPJ guides cold air southward, and the barrier effect of the powerful EASJ causes cold air to be enriched around the NE-N region. With the enhancement of the wave train in Eurasia at 500 hPa, the blockage situation makes the cold air accumulate to the east of the Ural Mountains and the west of Lake Baikal. The eastward-moving UBH at phase 7 and the stable downstream blocking high cause the NECV to contract and move southward, jointly with the strong SH on the SLP, leading to the northerly wind being enhanced. During this process, the cold air in the upper troposphere propagates southward and downward to the lower level, eventually resulting in the ECEs in the NE-N region.

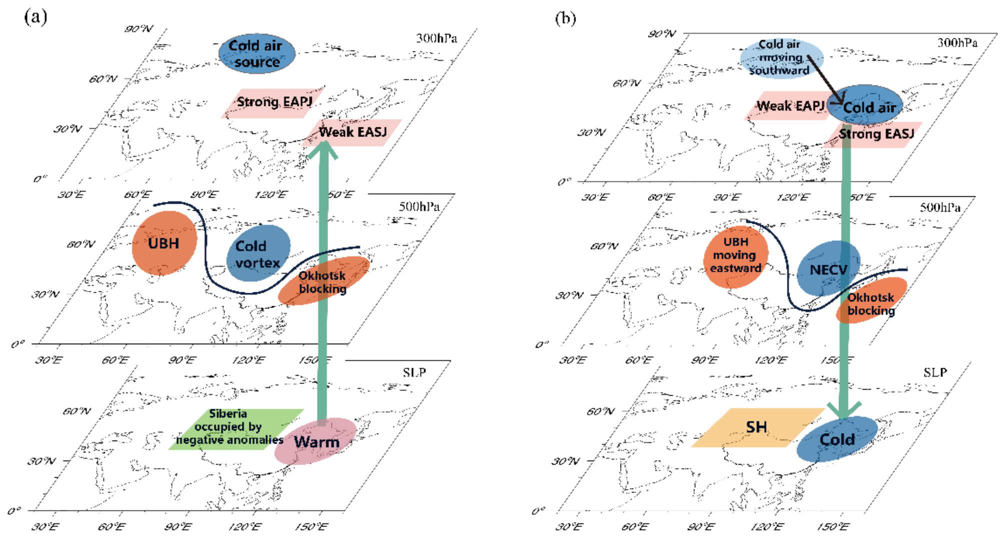

Figure 11. Schematic diagram of the configuration of the circulation systems in the (**a**) early stage and (**b**) later stage of LECEs.

6. Conclusions and Discussion

6.1. Conclusions

In this paper, we identify the key systems by analyzing the circulation characteristics of LECEs during the winter of 1979–2018, and the synergistic effects of the circulation systems on LECEs are discussed in conjunction with intensity indexes. The main conclusions are as follows:

(1) The frequency of ECEs in the NE-N region has obvious interannual anomaly characteristics; the dominant ISO period of regional-averaged T_{min} is 10–30 d.

(2) During the cooling phases, a pair of southeastward cyclone–anticyclone and intensifying SH jointly induce anomalous northerly wind. A low-frequency wave train in the middle troposphere leads to the NECV developing with a blockage situation. The cold center expands and strengthens, accompanied by an extending downward and southward cold vortex. The upper troposphere is dominated by weak EAPJ and strong EASJ, guiding the cold air outbreak and accumulating in the NE-N region.

(3) The 200 hPa wave activity flux shows north and south branch wave trains over the Eurasian region. The north one indicates a "+ − +" wave train, which moves southeastward through the Ural Mountains and Lake Baikal to the East Asian coast. Over the NE-N region, there is a wave flux convergence zone in phases 6–7, and the NECV maintains due to the upstream energy replenishment. The south one, which reflects a weaker northwardly dispersed wave activity flux, enhances NECV in phases 2–6.

(4) The key circulation systems affecting LECEs include the SH, the UBH, the NECV, and the EASJ. The cold air locates near Novaya Zemlya in the early phases with weak systems. Subsequently, the developing UBH and stable Okhotsk Sea Blocking High induce the strongest NECV in phase 6. The SH in phase with the low temperature gradually extends and moves southward, and cooperates with the weak EAPJ and strong EASJ in phases 7–8 to account for cold air stagnation and ECEs over NE-N.

6.2. Discussion

It is worth noting that this paper only analyzes the circulation characteristics of the tropospheric atmosphere and the synergy of key systems during the ECEs. In fact, changes in the stratospheric atmosphere also have an important impact on the low temperature process. We notice that cold vortex and cold anomaly are initially located in the stratosphere, and then gradually descended (Figure 8); this characteristic is also reflected in other studies of low-temperature events in China [55,56]. Recent views examine that the influence of the stratosphere–troposphere coupling processes on the East Asian winter temperature is considerable [57]. The stratospheric polar vortex contains information that can enhance forecasts of cold air outbreaks [58]. The atmospheric circulation and dynamical characteristics of strong and weak stratosphere polar vortexes are also different [59]. Therefore, the contribution of the stratospheric system to ECEs will be demonstrated in the future. Equally, the propagation characteristics of low-frequency cold air in the stratosphere also need to be further explored.

Author Contributions: Conceptualization and methodology, Q.G.; data curation and visualization, L.W. and Y.L.; writing—original draft preparation, L.W. and Y.W.; writing—review and editing, Q.G. All authors have read and agreed to the published version of the manuscript.

Funding: This research was funded by the National Natural Science Foundation of China (Grant No., 42075032) and the National Key Research and Development Program of China (Grant No., 2018YFC1505804).

Institutional Review Board Statement: Not applicable.

Informed Consent Statement: Not applicable.

Data Availability Statement: NCEP-DOE Reanalysis 2 data can be found here: https://psl.noaa.gov/data/gridded/data.ncep.reanalysis2.html (accessed on 10 January 2022); the daily minimum temperature dataset is available from the authors.

Acknowledgments: We thank China Meteorological Data Network and National Centers for Environment Prediction /Department of Energy (NCEP/DOE) for providing datasets.

Conflicts of Interest: The authors declare no conflict of interest.

References

1. Song, L.; Wu, R. Combined Effects of the MJO and the Arctic Oscillation on the Intraseasonal Eastern China Winter Temperature Variations. *J. Clim.* **2019**, *32*, 2231–2295. [CrossRef]
2. Zhu, W.; Li, Q.; Wang, Z.; Shen, X. Climatological variability of cold air processes over China in recent 60 years. *Meteorol. Mon.* **2022**, *48*, 1–13. (In Chinese) [CrossRef]
3. Lan, K.; Li, T. The monsoon of East Asian and its global associations A Survey. *Bull. Am. Meteorol. Soc.* **1984**, *65*, 114–125. [CrossRef]
4. Guo, Q. Relationship between the variations of East Asian winter monsoon and temperature anomalies China. *J. Appl. Meteorol. Sci.* **1994**, *5*, 218–225. (In Chinese)
5. Yuan, C.; Li, W. Variations in the Frequency of Winter Extreme Cold Days in Northern China and Possible Causalities. *J. Clim.* **2019**, *32*, 8127–8141. [CrossRef]
6. Ma, F.; Chen, L.; Li, X.; Li, W.; Xu, B. Characteristics and Causes of Intraseasonal Variation of Winter Temperature in China under Different Interdecadal Scale. *Chin. J. Atmos. Sci.* **2022**, *46*, 573–589. (In Chinese)
7. Shen, H.; Ding, Y.; Zhang, J. Inter-decadal variations of winter air temperature in north China and its Circulation background. *J. Meteorol. Sci.* **2010**, *30*, 338–343. (In Chinese) [CrossRef]
8. Zhang, Y.; Zeng, H. Recent progresses in the studies of the East Asian jet streams. *J. Meteorol. Sci.* **2020**, *40*, 617–627. (In Chinese) [CrossRef]
9. Hu, S.; Li, Y.; Fang, C.; Chen, Z. The relationship between Ural blocking, Siberia high and the East Asian winter monsoon. *J. Lanzhou Univ. Nat. Sci.* **2018**, *54*, 440–452. (In Chinese) [CrossRef]
10. Li, Y.; Wang, J.; Wang, S. The integrated circulation anomalies of polar vortex, blocking and the Siberian high over the extreme low-temperature events. *J. Lanzhou Univ. Nat. Sci.* **2019**, *55*, 51–63. (In Chinese) [CrossRef]
11. Scherrer, S.C.; Croci-Maspoli, M.; Schwierz, C.; Appenzeller, C. Two-dimensional indices of atmospheric blocking and their statistical relationship with winter climate patterns in the Euro-Atlantic region. *Int. J. Climatol.* **2010**, *26*, 233–249. [CrossRef]
12. Chen, W.; Yang, S.; Huang, R. Relationship between stationary planetary wave activity and the East Asian winter monsoon. *J. Geophys. Res. Atmos.* **2005**, *110*, D14110. [CrossRef]
13. Wang, L.; Huang, R.; Gu, L.; Chen, W.; Kang, L. Interdecadal Variations of the East Asian Winter Monsoon and Their Association with Quasi-Stationary Planetary Wave Activity. *J. Clim.* **2009**, *22*, 4860–4872. [CrossRef]
14. Chen, W.; Kang, L. Linkage Between the Arctic Oscillation and Winter Climate over East Asia on the Interannual Timescale: Roles of Quasi-Stationary Planetary Waves. *Chin. J. Atmos. Sci.* **2006**, *30*, 863–870. (In Chinese)
15. Dong, W. Relationship between the high-latitude concurrent blocking in Northern Hemisphere winter and extreme cold events in China. Master's Thesis, Nanjing University of Information Science & Technology, Nanjing, China, 2021. (In Chinese) [CrossRef]

16. Tan, G.; Zhang, W. The 10-30d low-frequency variation of winter surface air temperature in China and its relationship with Ural mountain circulation. *Trans. Atmos. Sci.* **2018**, *41*, 502–512. (In Chinese) [CrossRef]
17. Yang, S.; Wu, B.; Zhang, R.; Zhou, S. The zonal propagating characteristics of low-frequency oscillation over the Eurasian mid-high latitude in boreal summer. *Sci. China Earth Sci.* **2013**, *56*, 1566–1575. [CrossRef]
18. Madden, R.A.; Julian, P.R. Description of a 40-50day oscillation of the zonal wind in the tropical Pacific. *J. Atmos. Sci.* **1971**, *28*, 702–708. [CrossRef]
19. Murakami, M. Analysis of the deep convective activity over the western Pacific and Southeast Asia. Part II: Seasonal and intraseasonal variation during the northern summer. *J. Meteorol. Soc. Jpn.* **1984**, *62*, 88–108. [CrossRef]
20. Chang, C.P.; Lim, H. Kelvin Wave-CISK: A Possible Mechanism for the 30-50 Day Oscillations. *J. Atmos. Sci.* **1988**, *45*, 1709–1720. [CrossRef]
21. Anderson, J.R.; Rosen, R.D. The latitude-height structure of 40-50day variations in atmospheric angular momentum. *J. Atmos. Sci.* **1983**, *40*, 1584–1591. [CrossRef]
22. Kikuchi, K.; Wang, B. Global perspective of the quasi-biweekly oscillation. *J. Clim.* **2009**, *22*, 1340–1359. [CrossRef]
23. Chan, J.C.; Ai, W.; Xu, J. Mechanisms responsible for the maintenance of the 1998 South China Sea summer monsoon. *J. Meteorol. Soc. Jpn.* **2002**, *80*, 1103–1113. [CrossRef]
24. Teng, H.; Branstator, G.; Wang, H.; Meehl, G.A.; Washington, W. Probability of US heat waves affected by a subseasonal planetary wave pattern. *Nat. Geosci.* **2013**, *6*, 1056–1061. [CrossRef]
25. Watanabe, T.; Yamazaki, K. The upper-level circulation anomaly over central Asia and its relationship to the Asian monsoon and mid-latitude wave train in early summer. *Clim. Dyn.* **2014**, *42*, 2477–2489. [CrossRef]
26. Takaya, K.; Nakamura, H. Mechanisms of intraseasonal amplification of the cold Siberian high. *J. Atmos. Sci.* **2005**, *62*, 4423–4440. [CrossRef]
27. Takaya, K.; Nakamura, H. Geographical dependence of upper-level blocking formation associated with intraseasonal amplification of the Siberian high. *J. Atmos. Sci.* **2005**, *62*, 4441–4449. [CrossRef]
28. Yang, S.; Zhu, Q. Oscillation and its relation to cold air activities in Asian winter. *Trans. Atmos. Sci.* **1990**, *13*, 339–347. (In Chinese) [CrossRef]
29. Qiu, M.; Lu, W.; Wang, S. ENSO episodes and low-frequency oscillation in the extra-tropical latitude of the northern hemisphere. *J. Trop. Meteorol.* **2006**, *22*, 454–460. (In Chinese) [CrossRef]
30. Hong, C.; Li, T. The extreme cold anomaly over Southeast Asia in February 2008: Roles of ISO and ENSO. *J. Clim.* **2009**, *22*, 3786–3801. [CrossRef]
31. Zhu, Y.; Jiang, J. The intraseasonal characteristics of wintertime persistent cold anomaly in China and the role of low frequency oscillation in the low latitude and midlatitude. *J. Trop. Meteorol.* **2013**, *29*, 649–655. (In Chinese) [CrossRef]
32. Ma, X.; Ding, Y.; Xu, H.; He, J. The relation between strong cold waves and low-frequency waves during the winter of 2004/2005. *Chin. J. Atmos. Sci.* **2008**, *32*, 380–394. (In Chinese)
33. Ren, J.; Zheng, J.; Xu, Y.; Tao, Y.; Zhang, W.; Ju, J. The intra-seasonal oscillation of Siberian High influenced on the winter temperature of Yunnan in 2007. *J. Yunnan Univ.* **2015**, *37*, 386–398. (In Chinese) [CrossRef]
34. Wei, L.; Chen, Q.; Xiong, G. The relationship between the geopotential height in stratosphere and the temperature of China in winter. *J. Chengdu Univ. Inf. Technol.* **2012**, *27*, 466–473. (In Chinese) [CrossRef]
35. Tong, J.; Ye, J.; Wei, L. Analysis on the Atmospheric Circulation and Low-Frequency Oscillation Characteristics of the Two Persistent Heavy Snow Processes over Yangtze and Huaihe River Valleys. *Plateau Meteorol.* **2019**, *38*, 845–855. (In Chinese)
36. Ma, N.; He, L.; Liang, S.; Guo, J. Low-frequency characteristics of winter-time cold air activity in the Beijing-Tianjin-Hebei region and the impacts of low-frequency variation of the Siberian High. *Acta. Geogr. Sin.* **2020**, *75*, 485–496. (In Chinese) [CrossRef]
37. Yuan, Z.; Yin, J.; Wei, M.; Yuan, Y. Spatio-Temporal Variations in the Temperature and Precipitation Extremes in Yangtze River Basin, China during 1961–2020. *Atmosphere* **2021**, *12*, 1423. [CrossRef]
38. Feng, Y.; Zhou, J.; Mo, L.; Yuan, Z.; Zhang, P.; Wu, J.; Wang, C.; Wang, Y. Long-Term Hydropower Generation of Cascade Reservoirs under Future Climate Changes in Jinsha River in Southwest China. *Water* **2018**, *10*, 235. [CrossRef]
39. Wu, X.; Wang, Z.; Zhou, X.; Lai, C.; Chen, X. Trends in temperature extremes over nine integrated agricultural regions in China, 1961–2011. *Theor. Appl. Climatol.* **2016**, *129*, 1279–1294. [CrossRef]
40. Kanamitsu, M.; Ebisuzaki, W.; Woollen, J.; Yang, S.-K.; Hnilo, J.J.; Fiorino, M.; Potter, G.L. NCEP-DOE AMIP-II Reanalysis (R-2). *Bull. Am. Meteorol. Soc.* **2002**, *83*, 1631–1644. [CrossRef]
41. Duchon, C.E. Lanczos Filtering in One and Two Dimensions. *J. Appl. Meteorol. Climatol.* **1979**, *18*, 1016–1022. [CrossRef]
42. Wu, H.; Wu, L. *Diagnosis and Prediction Method of Climate Variability*; China Meteorological Press: Beijing, China, 2005; pp. 208–225.
43. Huang, J. *Method of Meteorological Statistic Analysis and Forecasting*, 3rd ed.; China Meteorological Press: Beijing, China, 2004; pp. 297–299.
44. Wei, F. *Modern Climate Statistical Diagnosis and Prediction Techniques*, 2nd ed.; China Meteorological Press: Beijing, China, 2007; pp. 10–28.
45. Takaya, K.; Nakamura, H. A formulation of a phase-independent wave-activity flux for stationary and migratory quasigeostrophic eddies on a zonally varying basic flow. *J. Atmos. Sci.* **2001**, *58*, 608–627. [CrossRef]
46. Xie, Z.; Bueh, C. Cold vortex events over Northeast China associated with the Yakutsk-Okhotsk blocking. *Int. J. Climatol.* **2017**, *37*, 381–398. [CrossRef]

47. Li, C.; Gu, W. An analyzing study of the anomalous activity of blocking high over the Ural Mountains in January 2008. *Chin. J. Atmos. Sci.* **2010**, *34*, 865–874. (In Chinese)
48. Yang, S.; Wu, B.; Zhang, R.; Zhou, S. Propagation of low-frequency oscillation over Eurasian mid-high latitude in winter and its association with the Eurasian teleconnection pattern. *Chin. J. Atmos. Sci.* **2014**, *38*, 121–132. (In Chinese) [CrossRef]
49. Wang, N.; Xu, X.; Wang, Y.; Zhang, Y.; Wu, W. The influence of upper level jet streams in East Asia on climatic effects of Eurasian teleconnection pattern in the winter. *Chin. J. Atmos. Sci.* **2017**, *41*, 461–474. (In Chinese)
50. Peng, J.; Bueh, C. The definition and classification of extensive and persistent extreme cold events in China. *Atmos. Ocean. Sci. Lett.* **2011**, *4*, 281–286. [CrossRef]
51. Liu, M.; Li, Y.; Lu, C. Analysis of the characteristics and atmospheric circulation causes of two types of extreme cold events in winter in China. *Plateau Meteorol.* **2021**, *40*, 603–620. (In Chinese)
52. Shi, N.; Wang, X.; Tian, P. Interdecadal variations in persistent anomalous cold events over Asian mid-latitudes. *Clim. Dyn.* **2019**, *52*, 3729–3739. [CrossRef]
53. Xu, M.; Guan, Z.; Cai, Q. Spatial and temporal evolution features of cooling extremes in China during winter half year from 1960 to 2015. *J. Meteorol. Sci.* **2020**, *40*, 733–743. (In Chinese) [CrossRef]
54. Ye, D.; Zhang, Y. Association of concurrent variation between the East Asian polar front and subtropical jets with winter cold air activity in China. *Chin. J. Atmos. Sci.* **2014**, *38*, 146–158. (In Chinese) [CrossRef]
55. Zhang, Z.; Qian, W. Precursors of regional prolonged low temperature events in China during winter half year. *Chin. J. Atmos. Sci.* **2012**, *36*, 1269–1279. (In Chinese)
56. Wu, J.; Ren, R. Stratosphere–Troposphere Interactions during Nationwide Extensive and Persistent Extreme Cold Events in Boreal Winter. *Chin. J. Atmos. Sci.* **2021**, *45*, 558–572. (In Chinese)
57. Yu, Y.; Cai, M.; Shi, C.; Ren, R. On the Linkage among Strong Stratospheric Mass Circulation, Stratospheric Sudden Warming, and Cold Weather Events. *Mon. Weather. Rev.* **2018**, *146*, 2717–2739. [CrossRef]
58. Kolstad, E.W.; Breiteig, T.; Scaife, A.A. The association between stratospheric weak polar vortex events and cold air outbreaks in the Northern Hemisphere. *Q. J. R. Meteorol. Soc.* **2010**, *136*, 886–893. [CrossRef]
59. Ma, J.; Chen, W.; Lan, X. Comparative Analysis of the Evolution Processes of the Strong and Weak Stratosphere Polar Vortex Events in Boreal Winter. *Chin. J. Atmos. Sci.* **2020**, *44*, 726–747. (In Chinese) [CrossRef]